

Supplementary Information for

Anomalous restoration of sp^2 hybridization in graphene functionalization

Subin Chae,^{2,†} Thanh-Hai Le,^{2,†} Chul Soon Park,^{2,3} Yunseok Choi,² Semin Kim,² Unhan Lee,² Haney Lee,¹ Eunseo Heo,² Yoong Ahm Kim,^{1,2} Oh Seok Kwon,^{3,4,} and Hyeonseok Yoon^{1,2,*}*

¹Alan G. MacDiarmid Energy Research Institute & School of Polymer Science and Engineering, Chonnam National University, 77 Yongbong-ro, Gwangju 61186, South Korea

²Department of Polymer Engineering, Graduate School, Chonnam National University, 77 Yongbong-ro, Gwangju 61186, South Korea

³Infectious Disease Research Center, Korea Research Institute of Bioscience and Biotechnology (KRIBB), 125 Gwahak-ro, Daejeon 34141, South Korea

⁴Department of NanoBiotechnology, Korea University of Science and Technology (UST), 125 Gwahak-ro, Daejeon 34141, South Korea

[†]S.C. and L.T.-H. contributed equally.

Corresponding Authors:

*E-mail: oskwon79@kribb.re.kr, hyoon@chonnam.ac.kr

1. The full width at half maximum (FWHM) of the G peak

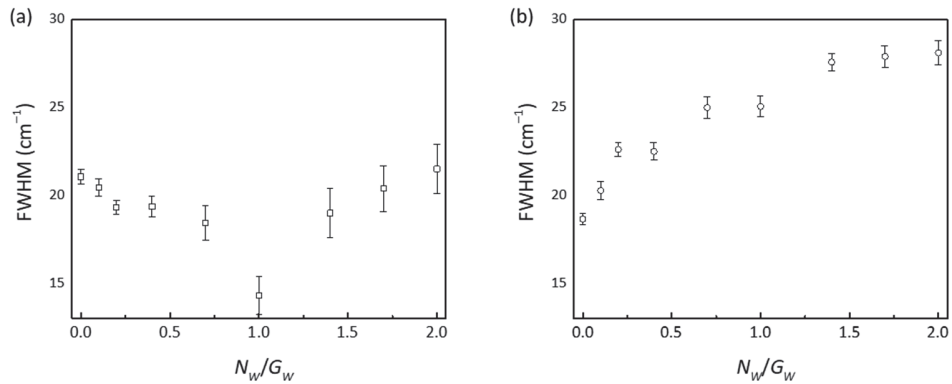


Figure S1. FWHM values of *G* peaks in the Raman spectra of (a) NHCp/G1 and (b) NHCp/G2 nanohybrids prepared with different N_w/G_w ratios.

2. X-ray photoelectron spectroscopy

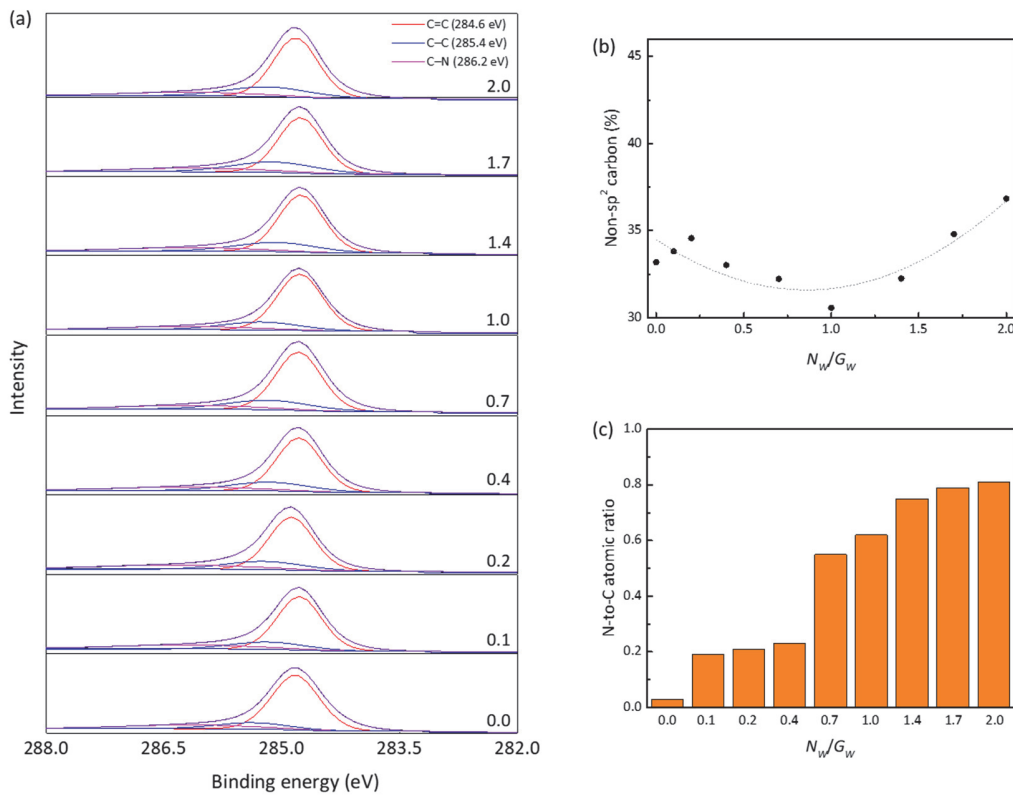


Figure S2. XPS analysis of NHCp/G1 nanohybrids prepared with different N_w/G_w ratios: (a) High-resolution C1s spectra (each spectrum was deconvoluted into three components) and (b) proportion of sp² graphitic carbon in the overall carbon content, calculated from the XPS spectra; (c) N/C atomic ratios.

Table S1. Deconvolution of C1s core-level XPS spectra of NHCp/G1 nanohybrids prepared with different N_w/G_w ratios.

NHCp/G1	Element	Functional groups	Binding energy (eV)	Atomic (%)
0.0	C1s	C=C	284.59	61.15
		C-C	285.38	18.33
		C-N	286.21	12.67
0.1	C1s	C=C	284.61	61.87
		C-C	285.39	18.25
		C-N	286.19	13.27
0.2	C1s	C=C	284.62	62.51
		C-C	285.41	17.68
		C-N	286.23	14.32
0.4	C1s	C=C	284.64	62.96
		C-C	285.39	16.64
		C-N	286.21	14.88
0.7	C1s	C=C	284.67	63.53
		C-C	285.42	15.76
		C-N	286.19	15.24
1.0	C1s	C=C	284.68	64.62
		C-C	285.18	13.71
		C-N	286.16	16.31
1.4	C1s	C=C	284.65	63.98
		C-C	285.41	13.96
		C-N	286.22	17.05
1.7	C1s	C=C	284.64	63.04
		C-C	285.43	14.05
		C-N	286.20	18.55
2.0	C1s	C=C	284.62	62.11
		C-C	285.38	14.77
		C-N	286.19	19.01

XPS was employed to obtain detailed information on the chemical structure of the NHCp/graphene nanohybrids. **Figure S2a** shows the high-resolution C1s spectra of NHCp/G1. A main component attributable to sp² carbon atoms was found at 284.6 eV. The two other peaks at 285.4 and 286.2 eV are ascribed to non-sp² carbon species such as nitrogenated and oxygenated carbon, respectively. The non-sp² carbon atoms act as defects in the graphene structure. **Figure S2b** displays the percentage of non-sp² carbon in the overall carbon content of the nanohybrids. The proportion of non-sp² carbon reached a minimum at $N_w/G_w = 1.0$, which is consistent with the I_D/I_G trend observed in the Raman data. The NHCp molecule has two nitrogen atoms that provide various functionalities. Therefore, the N/C atomic ratio may be representative of the amount of NHCp in the nanohybrids. As shown in **Figure S2c**, the N/C atomic ratio in the NHCp/G1 nanohybrids increased with increasing N_w/G_w ratio, indicating the incorporation of NHCp on/into the G1 pieces.

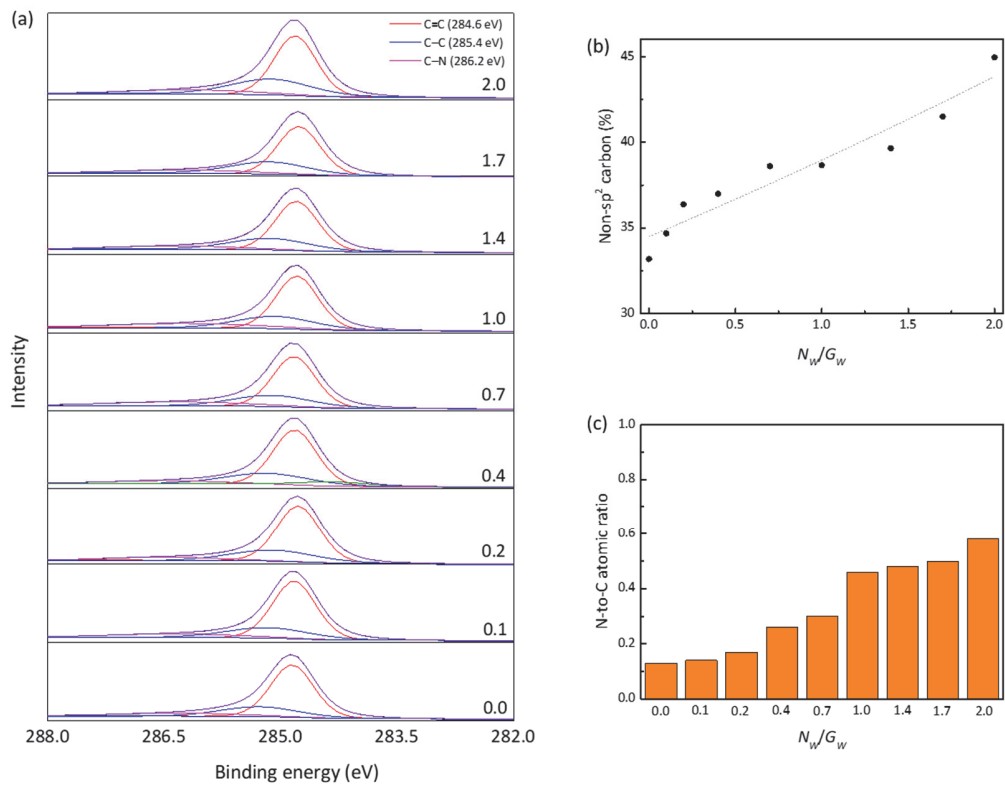


Figure S3. XPS analysis of NHCP/G2 nanohybrids prepared with different N_w/G_w ratios: (a) High-resolution C1s spectra (each spectrum was deconvoluted into three components) and (b) proportions of sp² graphitic carbon in the overall carbon content (the trend line is shown in red); (c) N/C atomic ratios.

Table S2. Deconvolution of C1s core-level XPS spectra of NHCp/G2 nanohybrids prepared with different N_w/G_w ratios.

NHCp/G2	Element	Functional groups	Binding energy (eV)	Atomic (%)
0.0	C1s	C=C	284.65	63.51
		C-C	285.27	22.79
		C-N	286.31	11.21
0.1	C1s	C=C	284.65	63.26
		C-C	285.27	23.31
		C-N	286.31	11.89
0.2	C1s	C=C	284.65	62.59
		C-C	285.27	23.56
		C-N	286.31	12.54
0.4	C1s	C=C	284.65	62.44
		C-C	285.27	23.65
		C-N	286.31	13.15
0.7	C1s	C=C	284.65	61.75
		C-C	285.27	22.28
		C-N	286.31	14.92
1.0	C1s	C=C	284.61	61.08
		C-C	285.12	22.05
		C-N	286.19	15.25
1.4	C1s	C=C	284.65	60.91
		C-C	285.27	22.65
		C-N	286.31	15.95
1.7	C1s	C=C	284.65	59.67
		C-C	285.27	24.55
		C-N	286.31	16.45
2.0	C1s	C=C	284.69	59.15
		C-C	285.07	26.54
		C-N	286.22	16.97

The NHCp/G2 nanohybrids were also characterized by XPS. As shown in **Figure S3a**, the C1s spectra were deconvoluted into the same three components (sp^2 , nitrogenated, and oxygenated carbons) as in **Figure S2a**. **Figure S3b** shows that the percentage of non- sp^2 carbons, indicative of the number of defects in graphene, increased with increasing N_w/G_w ratio. The trend of the non- sp^2 carbon proportion as a function of the N_w/G_w ratio was comparable to the I_D/I_G trend in the Raman data, for all N_w/G_w ratios except 1.7 and 2.0. It is expected that NHCp itself would contribute to the increase in the non- sp^2 carbon proportion at high N_w/G_w ratios (≥ 1.7). The N/C atomic ratio also increased with increasing N_w/G_w ratio, (**Figure S3c**), which was consistent with the trend observed for the NHCp/G1 nanohybrids. The trend of the N/C *vs.* N_w/G_w ratio in both **Figures S2c** and **S3c** was not linear. The introduction of NHCp onto/into graphene pieces would depend on the degree of graphene exfoliation. The NHCp molecules first attach to the edge of the G2 graphene sample and then occupy all available edge sites ($N_w/G_w \leq 0.7$). After further graphene exfoliation into separate pieces, NHCp can be introduced into the center of the graphene pieces, which enables the incorporation of additional NHCp molecules (N_w/G_w ratio ≥ 1.0).

3. Magnified Raman spectra showing the G' peaks

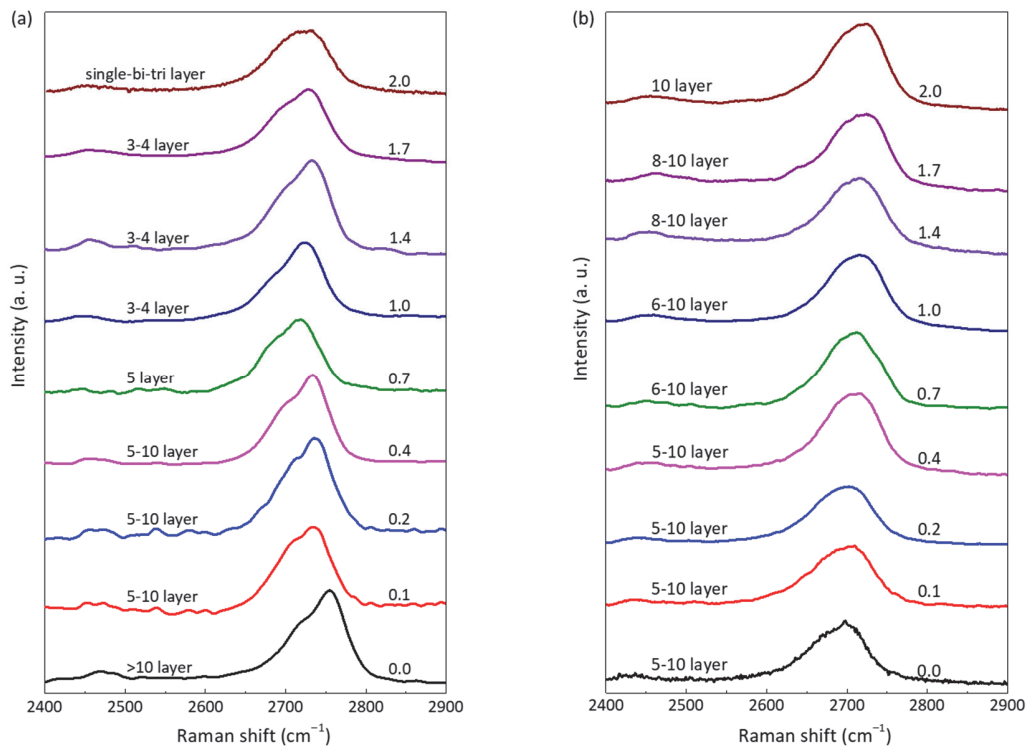


Figure S5. Raman spectra of (a) NHCp/G1 and (b) NHCp/G2 nanohybrids prepared with different N_w/G_w ratios, measured in the 2400–2900 cm^{-1} range.

4. Transmission electron microscopy/energy-dispersive X-ray spectroscopy

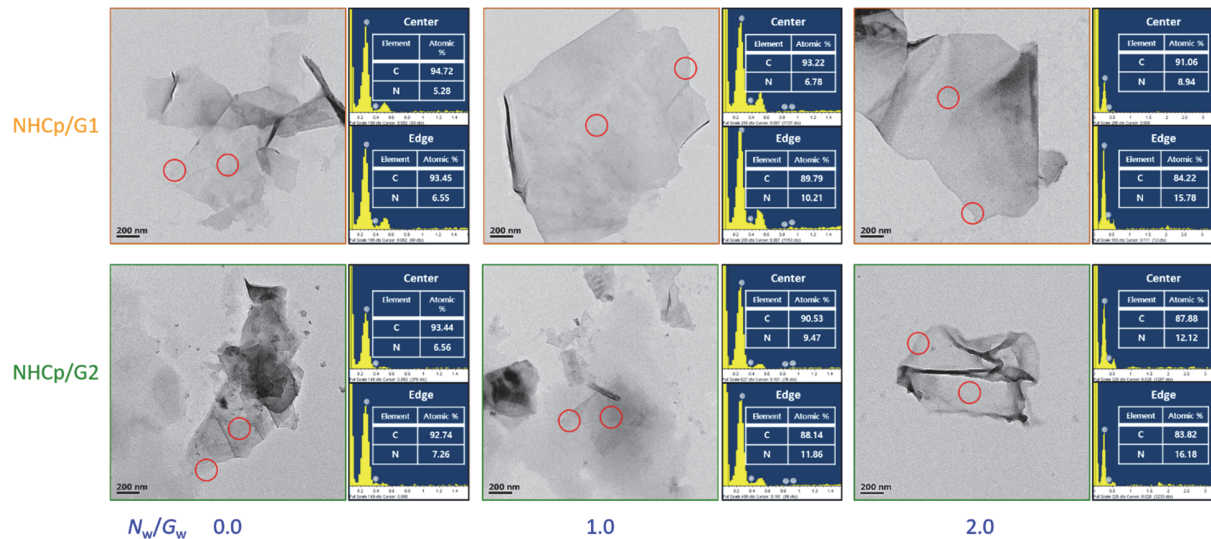


Figure S6. Transmission electron microscopy images and energy dispersive X-ray (EDX) spectra of NHCp/G1 and NHCp/G2 nanohybrids prepared with different N_w/G_w ratios. The red circles indicate the sites (namely, the center and the edge) selected for obtaining the EDX spectra.

5. Cyclic voltammetry

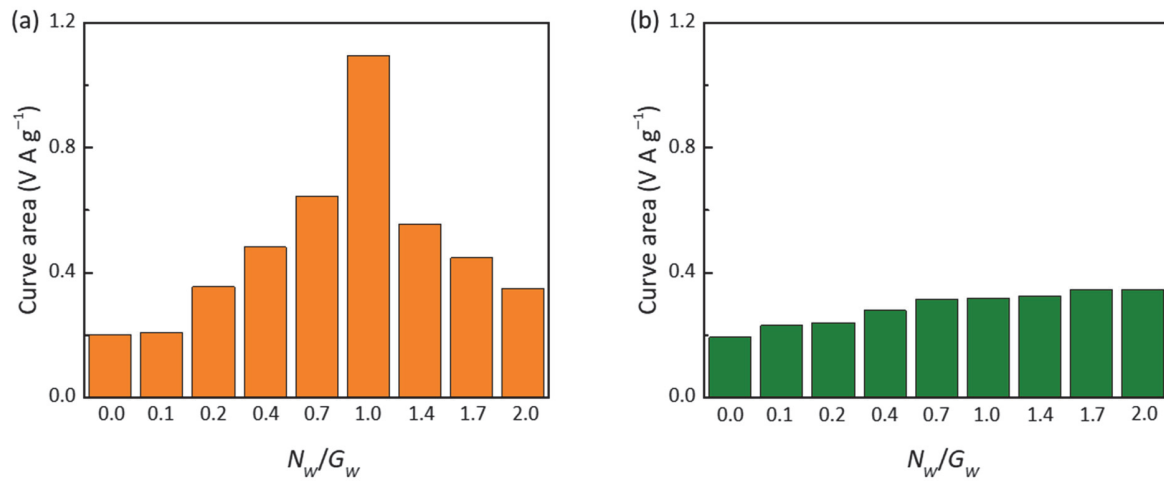


Figure S7. Integrated areas of CV curves of (a) NHCp/G1 and (b) NHCp/G2 nanohybrids prepared with different N_w/G_w ratios, shown in Figure 3.

6. Specific discharge capacitances

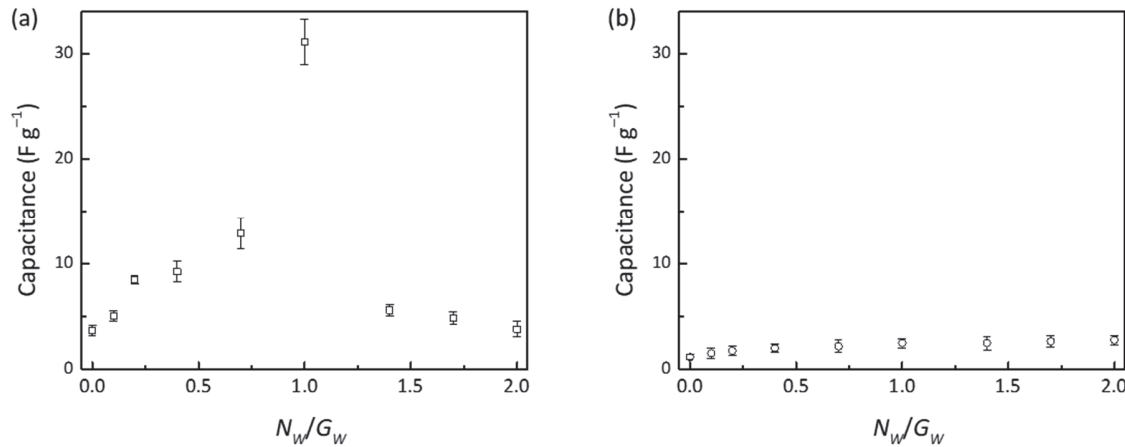


Figure S8. Discharge capacitance values of (a) NHCp/G1 and NHCp/G2 nanohybrids prepared with different N_w/G_w ratios, calculated from the charge/discharge curves shown in Figure 3.

Table S3. Main parameters calculated for the covalent attachment modes of NHCp^a to the three graphene models of different size.

Model		E_{graphene}	$E_{\text{carbene/graphene}}$	Binding energy
		(a.u.)	(a.u.)	(ΔE_b)
a)	C ₉₆	-3677.82	-4908.01	0.02
	C ₅₅	-2072.29	-3302.49	-0.01
	C ₂₄	-924.17	-2154.39	-0.04
b)	C ₉₆	-3677.82	-4908.01	-0.05
	C ₅₅	-2072.29	-3302.55	-0.05
	C ₂₄	-924.17	-2154.43	-0.05
c)	C ₉₆	-3677.82	-4908.06	-0.03
	C ₅₅	-2072.29	-3302.54	-0.04
	C ₂₄	-924.17	-2154.41	-0.03
d)	C ₉₆	-3677.82	-4908.05	-0.02
	C ₅₅	-2072.29	-3302.53	-0.03
	C ₂₄	-924.17	-2154.42	-0.04
e)	C ₉₆	-3677.82	-4908.10	-0.07
	C ₅₅	-2072.29	-3302.51	-0.01
	C ₂₄	-924.17	-2154.42	-0.04

^aThe absolute energy of NHCp was calculated to be -1230.21 a.u.

7. Density functional theory calculation

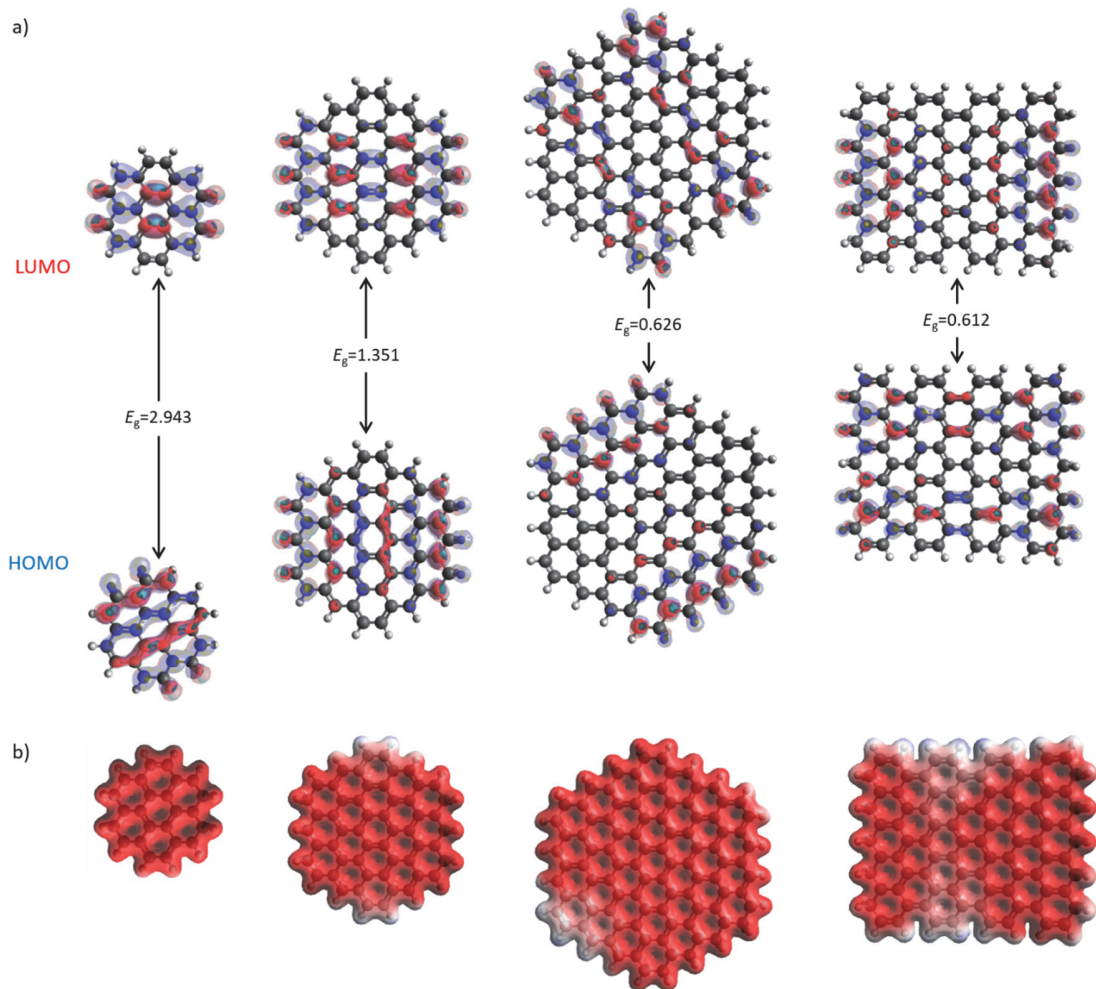


Figure S9. G_h models of three different sizes (C₂₄, C₅₄, and C₉₆) and G_t model (C₉₆): (a) Frontier molecular orbitals with bandgap energy values and (b) electron densities of the coupling models calculated at the B3LYP/6-31G(d) level of theory.

Table S4. Main calculated parameters for the covalent attachment modes of NHCp to the G_h edges (coupling models **1–4**), illustrated in Figure 5.^a

Model	E_{graphene} (a.u.)	$E_{\text{carbene/graphene}}$ (a.u.)	Binding energy (ΔE_b)
1	−3677.82	−4908.08	−0.05
2	−3677.82	−4908.06	−0.03
3	−3677.82	−4908.05	−0.02
4	−3677.82	−4908.10	−0.07

^aThe absolute energy of NHCp was calculated to be −1230.21 a.u.

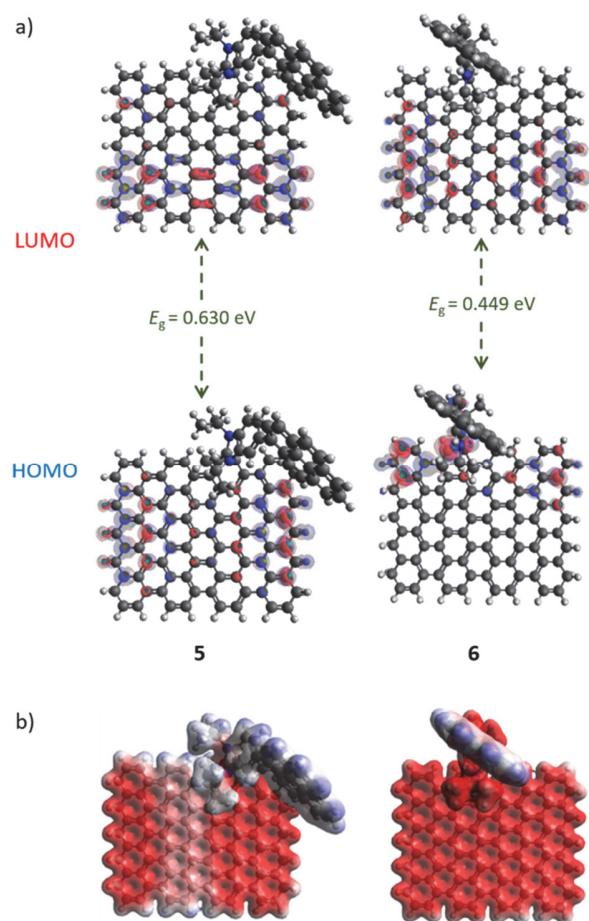


Figure S10. Covalent attachment of NHCp to the G_t edges (coupling models **5** and **6**): (a) Frontier molecular orbitals and bandgap energy values and (b) electron densities of the coupling models calculated at the B3LYP/6-31G(d) level of theory.

Table S5. Main calculated parameters calculated for the covalent attachment modes of NHCp to the G_t edges (coupling models **5** and **6**), illustrated in Figure S10.^a

Model	E_{graphene}	$E_{\text{carbene/graphene}}$	Binding energy
	(a.u.)	(a.u.)	(ΔE_b)
5	-3375.27	-4605.53	-0.05
6	-3375.27	-4605.52	-0.04

^aThe absolute energy of NHCp was calculated to be -1230.21 a.u.

Additional calculations were performed on another C₉₆ graphene model with armchair edge structure (tetragonal graphene, G_t) to further clarify the effect of the NHCp functionalization at the armchair edge. As shown in **Figure S10** (see also **Table S5**) the results of these calculations were consistent with those discussed above. In particular, the results confirmed that a single-covalent bond at the armchair edge contributed to the orbital hybridization and electron delocalization between NHCp and graphene. The bandgap energy also showed a marked decrease even after the single-covalent bond attachment. Calculations using another graphene model with zigzag edge structure showed similar results to those obtained with the G_h model. Therefore, it is reasonable to conclude that the covalent attachment of NHCp to the graphene edge, particularly the armchair-type edge, would not only affect the HOMO/LUMO energy levels (enhancing the electronic conductivity), but also alter the double resonance process, making the Raman *D* peak inactive.

8. Experimental Details

Materials. Graphite flakes (Sigma-Aldrich, 99%), anhydrous tetrahydrofuran (THF, Sigma-Aldrich, ≥99.9%), potassium bis(trimethylsilyl)amide (KHMDS, Sigma-Aldrich, 95%, 1 M in THF), and *N*-methyl-2-pyrrolidinone (NMP, Acros, ≥99.5%) were used as received, without further purification. 4-Bromo-2-nitroaniline (97%), pyrene-1-boronic acid (≥95.0%), Cs₂CO₃ (≥99.0%), palladium tetrakis(triphenylphosphine) (Pd(PPh₃)₄, Sigma-Aldrich, ≥99.99%), *N,N*-dimethylformamide (DMF, 99.8%), formic acid (≥95%), iron powder (≥99%), NH₄Cl (≥99.5%), isopropyl alcohol (≥98%), K₂CO₃ (99.995%), dichloromethane (≥99.8%), methanol (≥99.9%), NaHCO₃ (≥95%), Na₂SO₄ (≥99%), 2-iodopropane (99%), and acetonitrile (99.8%) were purchased from Sigma-Aldrich and used as received. Poly(vinylidene fluoride) (PVDF; KF13 binder) was used as a binder for fabricating the working electrodes.

Characterization. Raman spectra were recorded using a NanoBase XperRam 200 spectrophotometer with a 532 nm excitation source. Ultraviolet (UV)-visible spectra were obtained on an Opizzen 2120UV spectrometer, while X-ray photoelectron spectroscopy (XPS) measurements were performed with a Kratos AXIS-HSI spectrometer equipped with a high-performance Mg/Al X-ray excitation source. Scanning electron microscopy (SEM) measurements were conducted on a ZEISS Gemini 500 electron microscope.

Graphene samples. Two different approaches were used to prepare graphene samples G1 and G2. To prepare G1, graphite flakes (2 g) were added into a mixture of H₂SO₄, K₂SO₄, and P₂O₅ (50 mL/10 g/10 g) at 80 °C and stirred for 1 h. The mixture solution was filtered using a polytetrafluoroethylene (PTFE) membrane (0.2 μm pore size, Whatman); the obtained black powder was thoroughly washed with distilled water and then dried in vacuum at room temperature

for use as G1 precursor. The G1 precursor powder was dispersed in NMP solution (1.3 mg mL^{-1}) by 30 min ultrasonication (20 kHz, 25 kW L $^{-1}$, Sonics & Materials, Inc., USA) to yield the G1 graphene product. Next, in order to prepare G2, graphite flakes were added to the NMP solution (2.5 mg mL^{-1}), which was then subjected to mild sonication (40 kHz, 35 W L $^{-1}$, Powersonic 420, Hwashin Technol. Co., Korea) for 12 h. The obtained dispersion solution was centrifuged at 10,000 rpm for 30 min to remove bulky graphite fragments. Finally, the G2 graphene product was obtained after vacuum drying at room temperature.

Synthesis of NHCp and reaction with graphene.

- i) Synthesis of 2-nitro-4-(pyrenyl)aniline (NPA): 4-Bromo-2-nitroaniline (6.0 g, 27.6 mmol), pyrene-1-boronic acid (8.16 g, 33.2 mmol), Cs₂CO₃ (18.01 g, 55.3 mmol), and Pd(PPh₃)₄ (3.2 g, 2.76 mmol) were stirred in DMF (140 mL) at 100 °C for 12 h under argon atmosphere and then cooled down at room temperature. The solid byproduct was filtered off using a Celite pad and the filtrate solution was evaporated. The residue was then purified by silica column chromatography using ethyl acetate/n-hexane as eluent to afford the final product as an orange solid (4.38 g, yield 47%).
- ii) Synthesis of 5-(pyren-1-yl)-1*H*-benzo[*d*]imidazole (PBI): Formic acid (70 mL) was mixed with NPA (4.3 g, 12.7 mmol), iron powder (7.1 g, 127 mmol), and NH₄Cl (6.8 g, 127 mmol) in isopropyl alcohol (90 mL). The reaction mixture was stirred at 100 °C for 12 h under argon atmosphere and then cooled down to room temperature. The crude solid product was filtered off and the filtrate was then extracted using ethanol (300 mL). The filtrate solution was evaporated and the obtained residue was treated with K₂CO₃ (8.8 g, 63.7 mmol) in dichloromethane/methanol (8:1, v/v) binary

solvent and then filtered. The filtrate was washed with a saturated NaHCO_3 aqueous solution, followed by washing with brine/chloroform to extract only the organic layer. The organic extract was dried over Na_2SO_4 and concentrated to dryness. The crude product was treated with ether for 5 h. After removing the impurities-containing ether *via* filtration, a light yellow solid (2.63 g, yield 65%) was finally obtained.

iii) Synthesis of 1,3-diisopropyl-5-(pyrenyl)-1*H*-benzo[*d*]imidazolium iodide (BIp): PBI (800 mg, 2.51 mmol) was mixed with 2-iodopropane (6.3 mL, 62.8 mmol) and Cs_2CO_3 (818 mg, 2.51 mmol) in acetonitrile (125 mL) and then refluxed at 90 °C for 24 h with stirring. The reaction mixture was cooled down to room temperature and the solid residue was filtered off. The filtrate solution was evaporated and purified by silica column chromatography using dichloromethane/methanol as an eluent, to afford an ivory solid (670 mg, yield 50%).

iv) Reaction of NHCp with graphene: To obtain NHCp, BIp (4 mg) was first dissolved in THF (3 mL). Then, a 1 M potassium bis(trimethylsilyl)amide (KHMDS) solution (10 μL) was further diluted with THF (3 mL) and added dropwise as a strong base into the BIp THF solution, until reaching a final BIp/KHMDS molar ratio of 1:1. The mixture solution was stirred for 1 h under inert atmosphere. Reactive carbene molecules were added into a dispersion of graphene (G1 or G2) in NMP and vigorously stirred at 25 °C for 12 h, while controlling the NHCp:graphene weight ratio. The final products were harvested *via* purification processes such as filtering (0.2 μm pore size, Whatman) and washing, and then vacuum-dried at room temperature.

To confirm the identity of intermediates and products, ¹H and ¹³C nuclear magnetic resonance (NMR) spectra were recorded on a Varian Unity INOVA 600 MHz Fourier-transform (FT)-NMR spectrometer. Mass spectrometry (MS) measurements were performed with a Bruker micrOTOF-Q II spectrometer equipped with an electrospray ionization (ESI) interface. All NMR and MS data are provided in the Supporting Information (see Fig. S10 to S18).

Electrochemical measurements. Cyclic voltammetry (CV), galvanostatic charge-discharge, and electrochemical impedance spectroscopy (EIS) tests were carried out with a Metrohm Auto B.V. PGSTAT101 potentiostat/galvanostat. All electrochemical measurements were performed using a three-electrode setup with a 1 M H₂SO₄ electrolyte, a Pt counter electrode, and an Ag/AgCl (with saturated KCl) reference electrode. To fabricate the working electrodes, the samples were coated onto a stainless steel current collector *via* the PVDF binder.

Theoretical Calculations. Density functional theory (DFT) calculations were carried out using the Gaussian 09 software. Graphene models of different sizes, consisting of 24, 54, and 96 carbon atoms, were used in the calculations. Geometry optimizations were performed using the B3LYP functional combined with 6-31G(d) split-valence basis sets. Binding energy (ΔE_b) values were calculated as energy differences between the final coupling structure and its independent components, as follows:

$$\Delta E_b = E_{\text{hybrid}} - (E_{\text{carbene}} + E_{\text{graphene}})$$

where E_{hybrid} , E_{graphene} , and E_{carbene} are the absolute energies obtained for the carbene/graphene hybrid, carbene, and graphene models after geometry optimization.

9. Supplementary data for the synthesis of NHCp

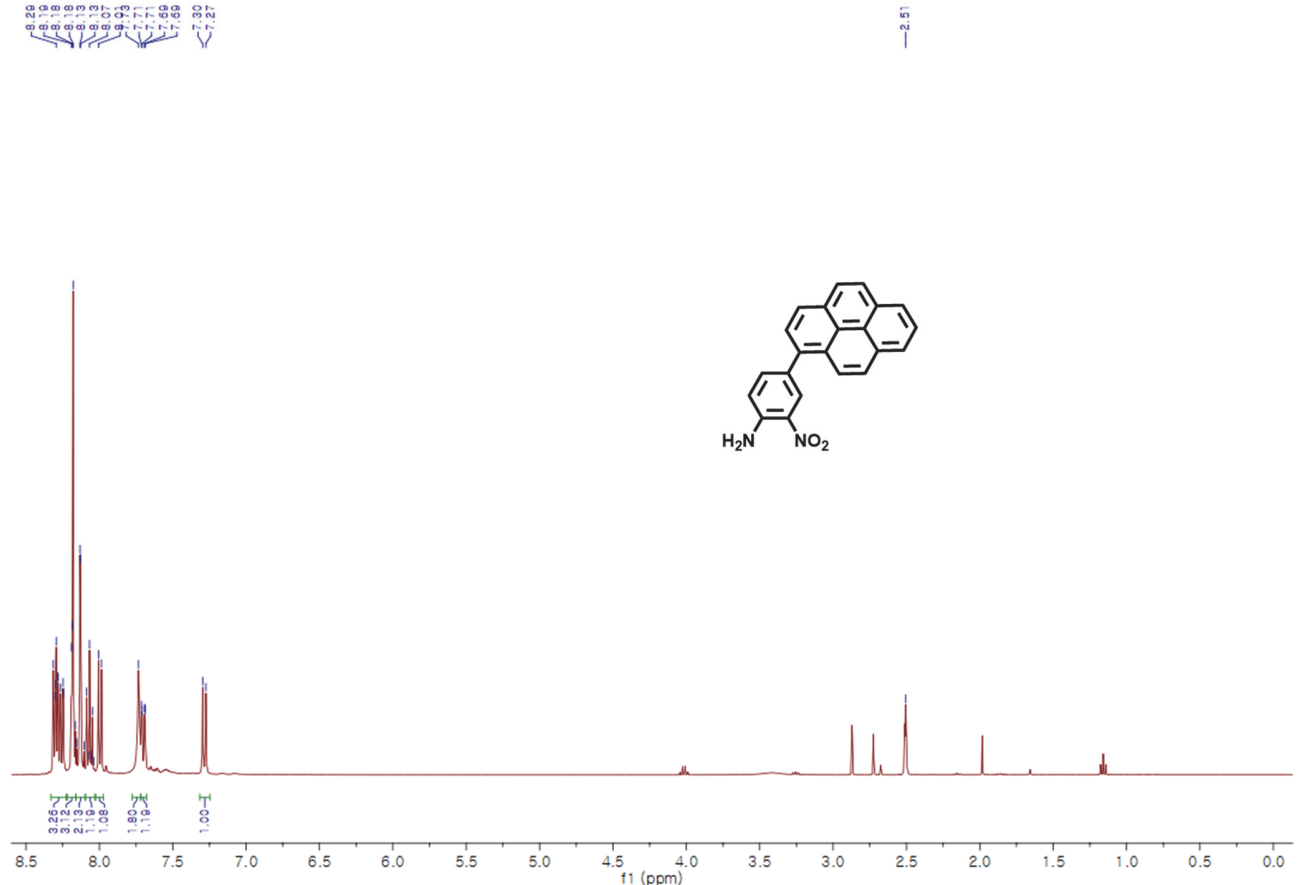


Figure S11. ¹H NMR spectrum of 2-nitro-4-(pyrenyl)aniline (NPA).

¹H NMR (400 MHz, DMSO) δ 8.33–8.23 (m, 3H), 8.22–8.16 (m, 3H), 8.16–8.10 (m, 2H), 8.06 (td, *J* = 7.9, 4.5 Hz, 1H), 8.00 (d, *J* = 7.9 Hz, 1H), 7.73 (s, 2H), 7.70 (dd, *J* = 8.7, 2.1 Hz, 1H), 7.29 (d, *J* = 8.7 Hz, 1H).

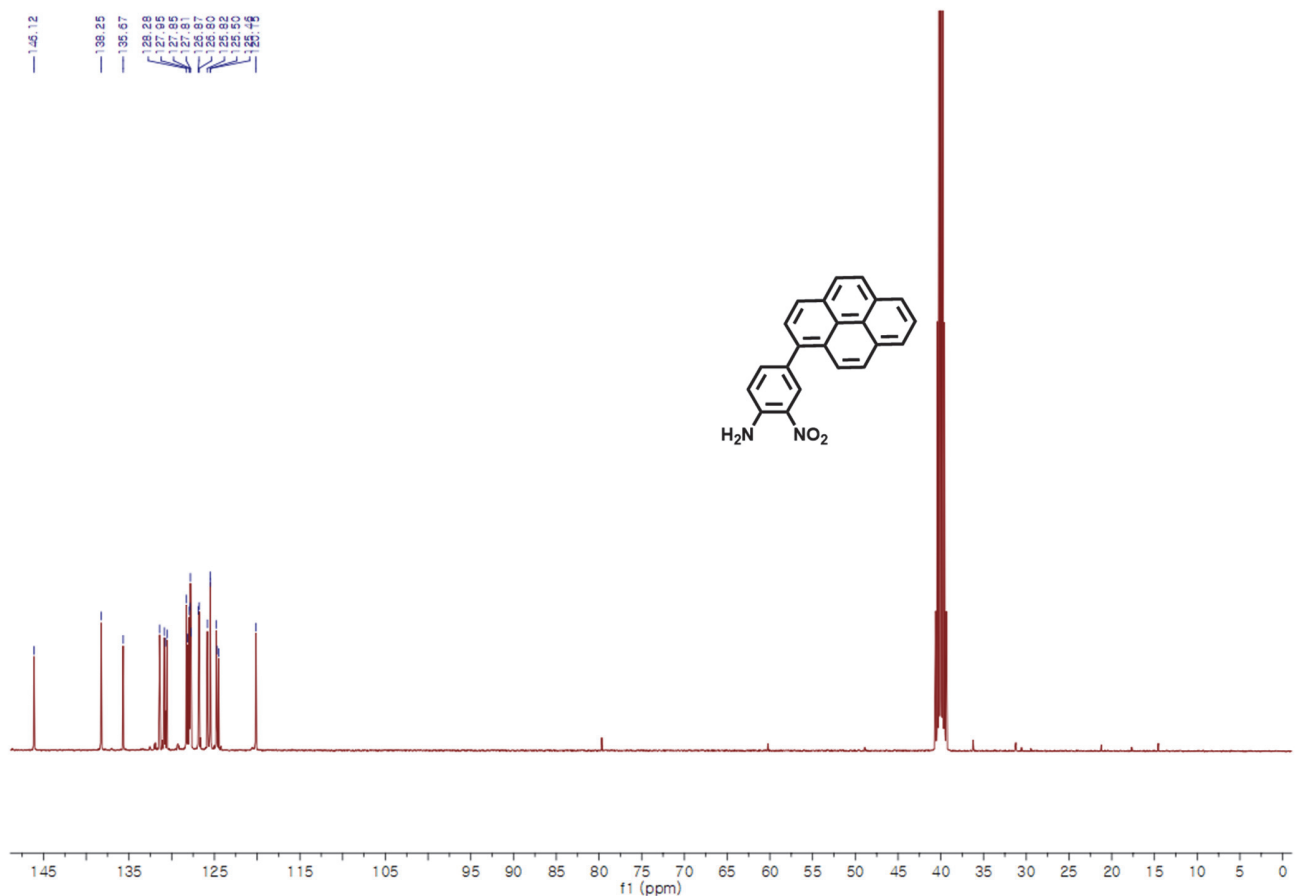


Figure S12. ^{13}C NMR spectrum of 2-nitro-4-(pyrenyl)aniline (NPA).

^{13}C NMR (100 MHz, DMSO) δ 146.12, 138.25, 135.67, 128.28, 127.95, 127.85, 127.81, 126.87, 126.80, 125.82, 125.50, 125.46, 120.15

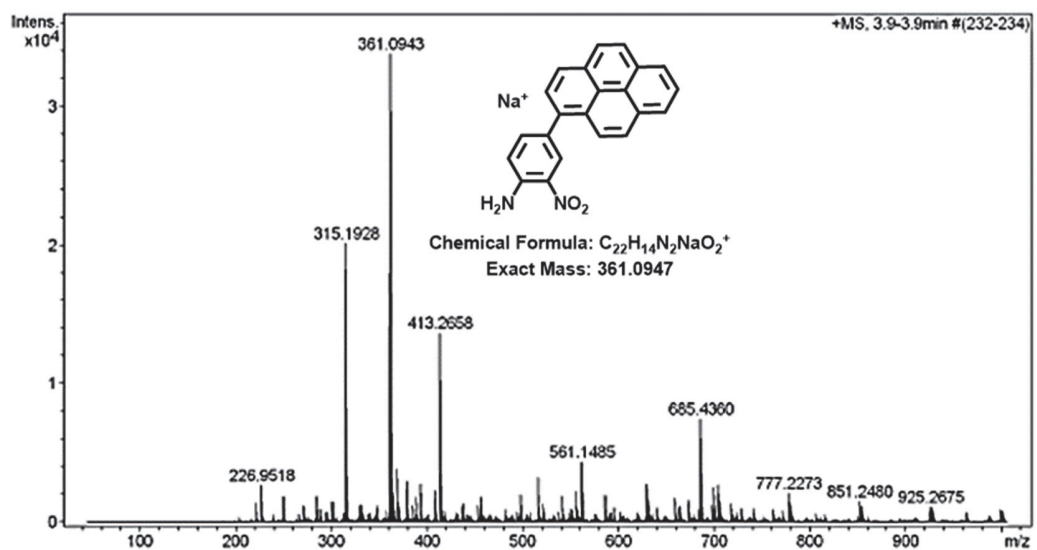


Figure S13. Mass spectrum of 2-nitro-4-(pyrenyl)aniline (NPA).

HRMS (TOF MS ES⁻) m/z calcd. for C₂₂H₁₄N₂NaO₂⁺(M–Na⁺): 361.0947. Found: 361.0943

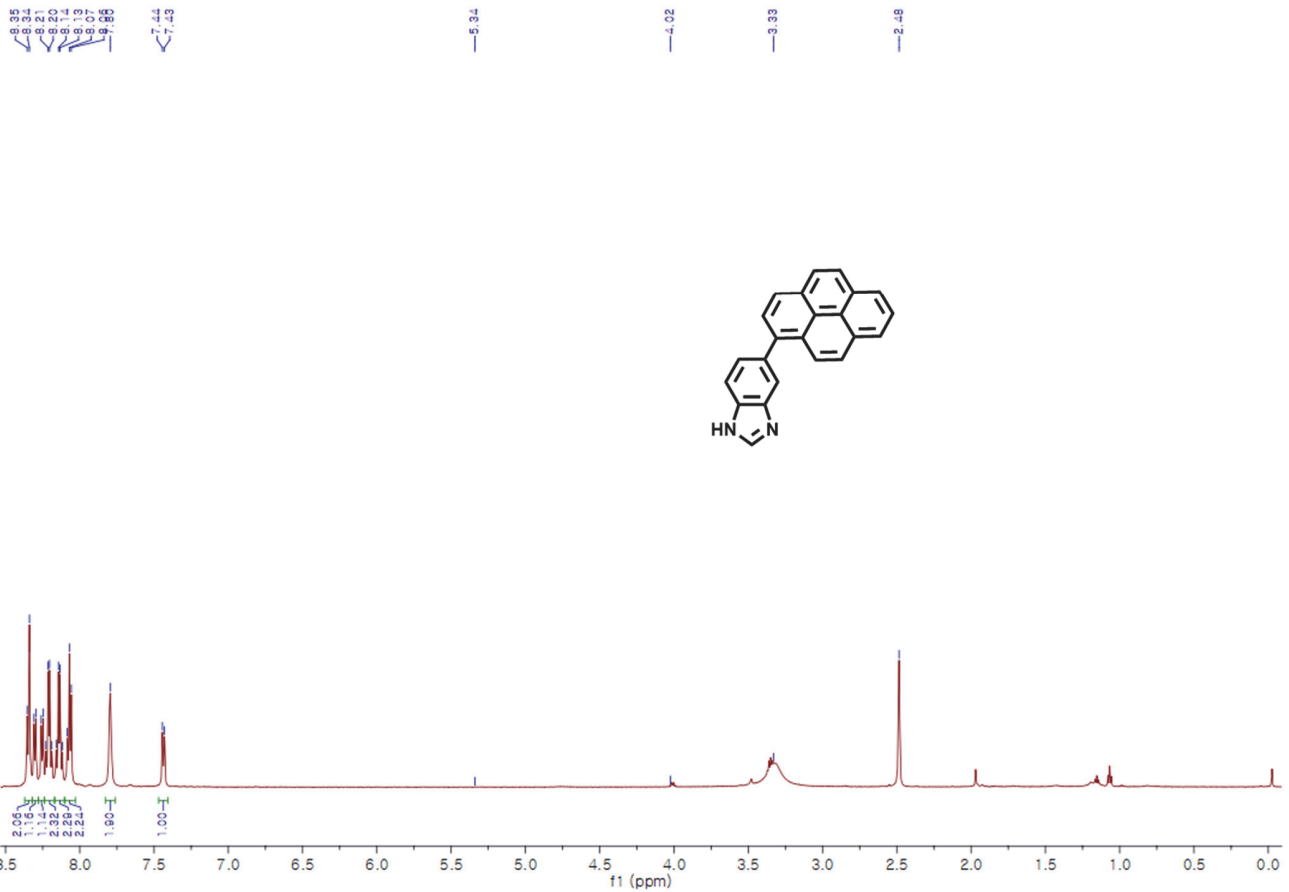


Figure S14. ¹H NMR spectrum of 5-(pyren-1-yl)-1*H*-benzo[*d*]imidazole (PBI).

¹H NMR (400 MHz, DMSO) δ 8.35–8.34 (m, 2H), 8.31–8.30 (d, *J* = 4.8 Hz, 1H), 8.26–8.25 (d, *J* = 5.2 Hz, 1H), 8.23–8.19 (dd, *J* = 10.0, 6.0 Hz, 2H), 8.16–8.12 (dd, *J* = 10.4, 6.0 Hz, 2H), 8.08–8.06 (t, *J* = 5.6 Hz, 2H), 7.80 (s, 2H), 7.44–7.43 (d, *J* = 5.6 Hz, 1H)

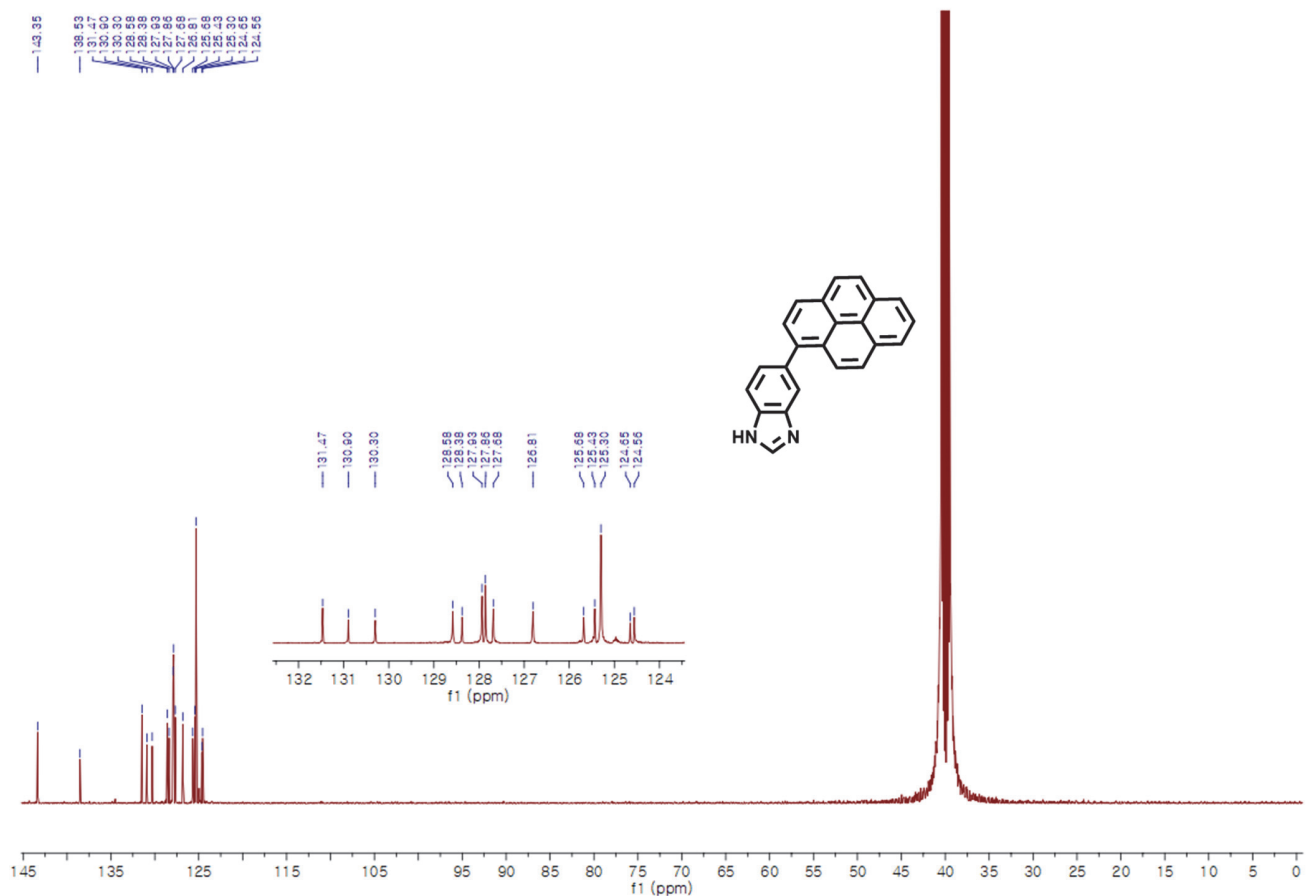


Figure S15. ^{13}C NMR spectrum of 5-(pyren-1-yl)-1*H*-benzo[*d*]imidazole (PBI).

^{13}C NMR (100 MHz, DMSO) δ 138.53, 131.47, 130.90, 130.30, 128.58, 128.38, 127.93, 127.86, 127.68, 126.81, 125.68, 125.43, 125.30, 124.65, 124.56

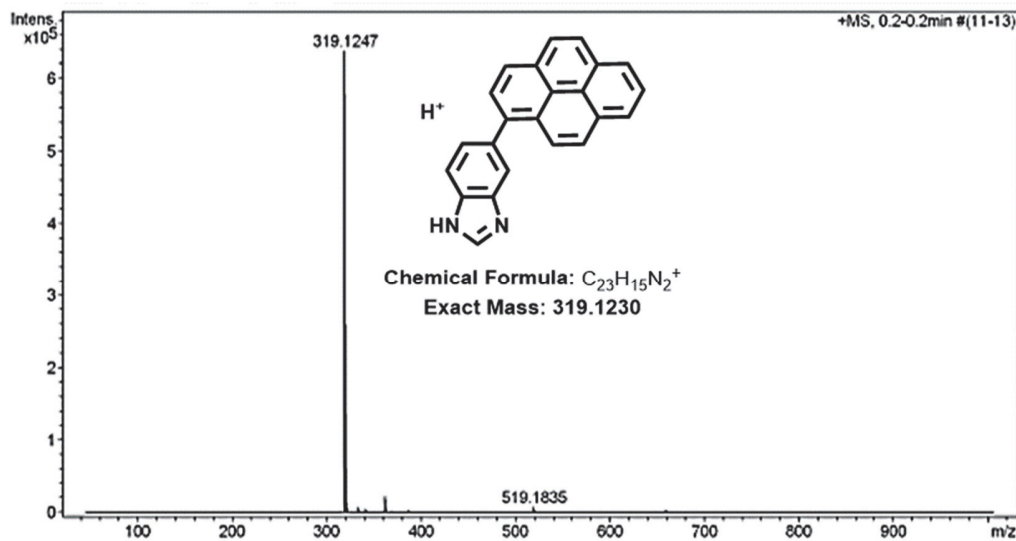


Figure S16. Mass spectrum of 5-(pyren-1-yl)-1*H*-benzo[*d*]imidazole (PBI).

HRMS (TOF MS ES⁻) *m/z* calcd. for $C_{23}H_{15}N_2^+(M-H^+)$: 319.1230. Found: 319.1247.

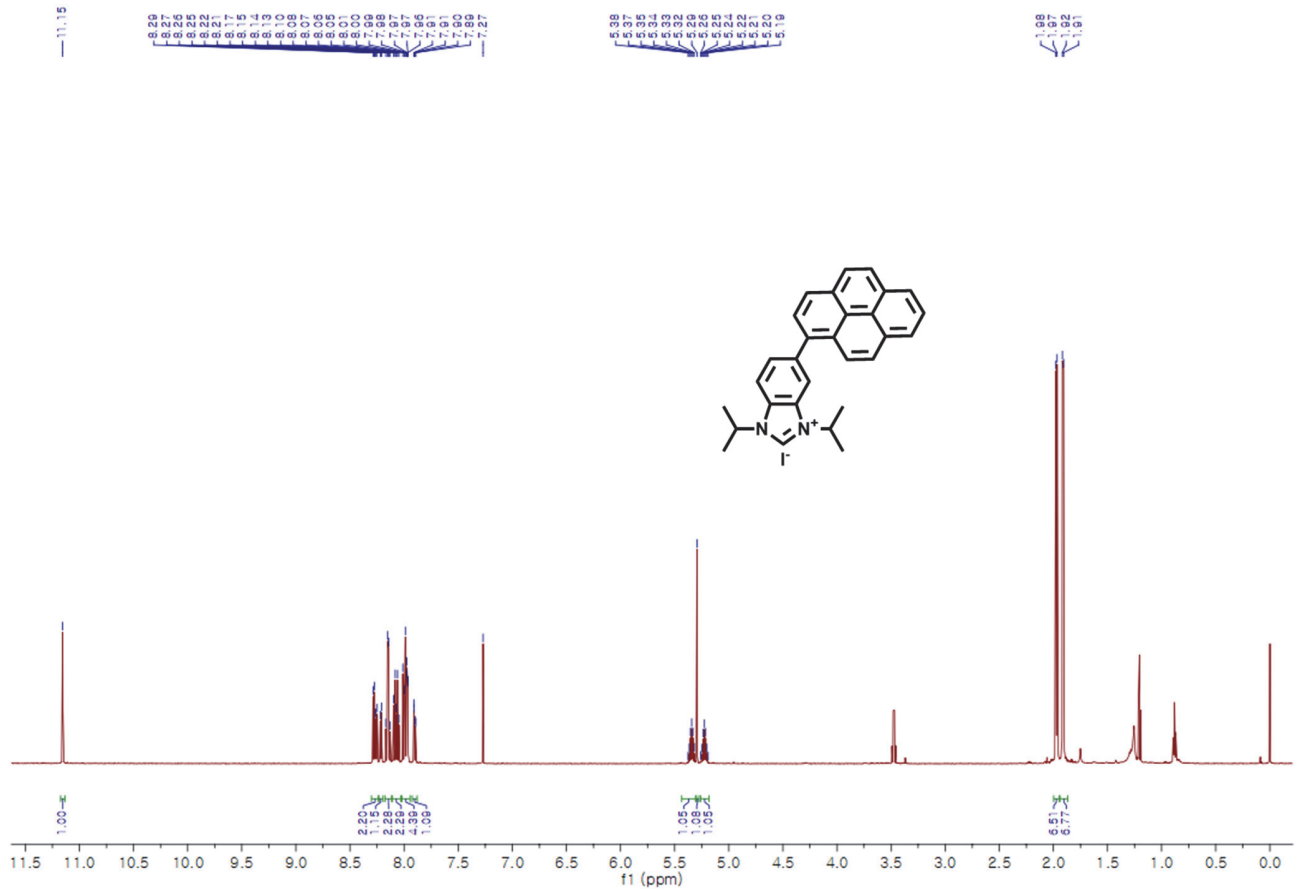


Figure S17. ¹H NMR spectrum of 1,3-diisopropyl-5-(pyrenyl)-1H-benzo[d]imidazolium iodide (BIP).

¹H NMR (400 MHz, CDCl₃) δ 11.15 (s, 1H), 8.29–8.25 (m, 2H), 8.22–8.21 (d, J = 4.8 Hz, 1H), 8.17–8.13 (dd, J = 10.4, 6.0 Hz, 2H), 8.10–8.05 (m, 2H), 8.01–7.96 (m, 4H), 7.91–7.89 (dd, J = 5.6, 0.8 Hz, 1H), 5.38–5.32 (m, 1H), 5.29 (s, 1H), 5.26–5.19 (m, 1H), 1.98–1.97 (d, J = 4.4, 6H), 1.92–1.91 (d, J = 4.4, 6H)

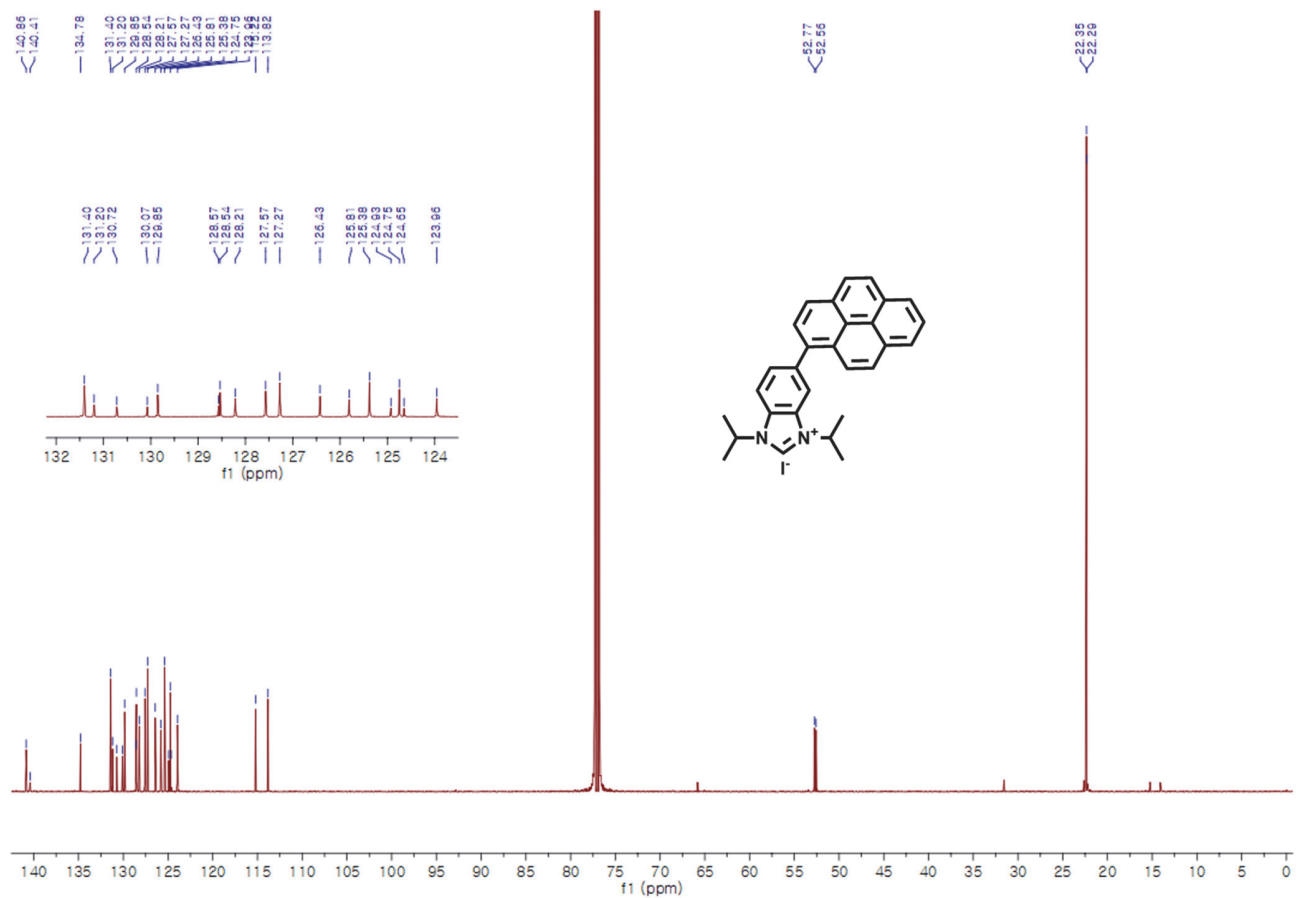


Figure S18. ^{13}C NMR spectrum of 1,3-diisopropyl-5-(pyrenyl)-1*H*-benzo[*d*]imidazolium iodide (BIP).

^{13}C NMR (100 MHz, CDCl_3) δ 140.86, 140.41, 134.78, 131.40, 131.20, 130.72, 130.07, 129.85, 128.57, 128.54, 128.21, 127.57, 127.27, 126.43, 125.81, 125.38, 124.93, 124.75, 124.65, 123.96, 115.22, 113.82, 52.77, 52.56, 22.35, 22.29

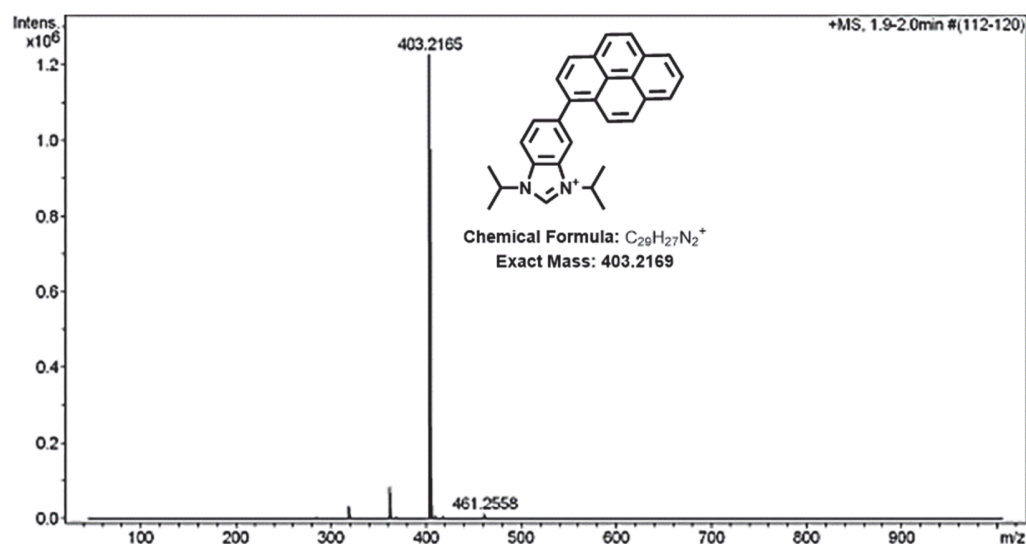


Figure S19. Mass spectrum of 1,3-diisopropyl-5-(pyrenyl)-1*H*-benzo[*d*]imidazolium iodide (BIP).

HRMS (TOF MS ES⁻) m/z calcd. for $C_{29}H_{27}N_2^+$: 403.2169. Found: 403.2165